1-1-2013

Optical solitary waves in thermal media with non-symmetric boundary conditions

Simon Louis
University of Wollongong, sal09@uowmail.edu.au

Timothy R. Marchant
University of Wollongong, tim@uow.edu.au

Noel F. Smyth
University of Wollongong

Optical solitary waves in thermal media with non-symmetric boundary conditions

Abstract

Optical spatial solitary waves are considered in a nonlocal thermal focusing medium with non-symmetric boundary conditions. The governing equations consist of a nonlinear Schrödinger equation for the light beam and a Poisson equation for the temperature of the medium. Three numerical methods are investigated for calculating the ground and excited solitary wave solutions of the coupled system. It is found that the Newton conjugate gradient method is the most computationally efficient and versatile numerical technique. The solutions show that by varying the ambient temperature, the solitary wave is deflected towards the warmer boundary. Solitary wave stability is also examined both theoretically and numerically, via power versus propagation constant curves and numerical simulations of the governing partial differential equations. Both the ground and excited state solitary waves are found to be stable. The Newton conjugate gradient method should also prove extremely useful for calculating solitary waves of other related optical systems, which support nonlocal spatial solitary waves, such as nematic liquid crystals. © 2013 IOP Publishing Ltd.

Keywords

media, non, symmetric, boundary, optical, conditions, solitary, waves, thermal

Disciplines

Engineering | Science and Technology Studies

Publication Details

Louis, S., Marchant, T. R. & Smyth, N. F. (2013). Optical solitary waves in thermal media with non-symmetric boundary conditions. Journal of Physics A: Mathematical and Theoretical, 46 (5), 055201-1-055201-21.

Optical solitary waves in thermal media with non-symmetric boundary conditions

S.A. Louis[1], **T.R. Marchant**[1], **and N.F. Smyth**[1]

[1] School of Mathematics and Applied Statistics,
The University of Wollongong,
Wollongong, 2522, N.S.W., Australia.

E-mail: sal09@uow.edu.au, tim_marchant@uow.edu.au, N.Smyth@ed.ac.uk

PACS numbers: 42.65.Tg, 42.70.Nq, 02.60.Pn

Abstract. Optical spatial solitary waves are considered in a nonlocal thermal focusing medium with non-symmetric boundary conditions. The governing equations consist of a nonlinear Schrödinger equation for the light beam and a Poisson equation for the temperature of the medium. Three numerical methods are investigated for calculating the ground and excited solitary wave solutions of the coupled system. It is found that the Newton conjugate gradient method is the most computationally efficient and versatile numerical technique. The solutions show that by varying the ambient temperature, the solitary wave is deflected towards the warmer boundary. Solitary wave stability is also examined both theoretically and numerically, via power versus propagation constant curves and numerical simulations of the governing partial differential equations. Both the ground and excited state solitary waves are found to be stable. The Newton conjugate gradient method should also prove extremely useful for calculating solitary waves of other related optical systems, which support nonlocal spatial solitary waves, such as nematic liquid crystals.

1. Introduction

The transmission of optical solitary waves is possible in a number of nonlinear media, such as glasses [1, 2, 3], nematic liquid crystals [4], thermal media [5, 6, 7, 8, 9, 10], photorefractive crystals and other bulk media [3] for which there is a balance between the diffraction (dispersion) and nonlinearity of the medium. These media have a refractive index which depends in a nonlinear fashion on the power of the optical beam, the precise response depending on the type of medium. For instance, in a thermal media the refractive index changes due to it absorbing thermal energy from the optical beam, while in a liquid crystal the refractive index changes due to molecular rotation caused by the electric field of the input beam. While, in principal, the refractive index of the medium can change due to a combination of effects, experimental operating conditions are controlled so that the dominant change in refractive index is due to a single effect. In addition, thermal effects are undesirable in media such as liquid crystals as temperature changes cause the medium to change state [11]. In such materials the refractive index of the material undergoes a nonlinear response that leads to the self-focusing of the light beam, counterbalancing its natural diffraction (dispersion). For some media, the response of the material to the light beam extends far beyond the beam, as measured by its width, termed waist in optical applications [4, 12], the response then being termed nonlocal. This nonlocal response is due to the nonlinear optical response of the medium being coupled to a diffusive-type equation, which is elliptic when time dependence is neglected [13]. This elliptic medium response means that the medium responds over the entire domain, not just in the vicinity of the optical beam. The nonlocal response also arrests the usual catastrophic collapse of (2+1)-D solitary waves governed by nonlinear Schrödinger-type (NLS) equations [3, 4, 12, 14, 15].

Two important classes of optical materials, which support nonlocal spatial optical solitary waves, are nematic liquid crystals [4, 12] and nonlinear thermal media [8]. A nematic liquid crystal is a material consisting of rod shaped organic molecules which exhibit orientational, but not positional order, and which can rotate under the influence of an electric field due to the electric field inducing a dipole in the molecules. This rotation increases the refractive index, so that self-focusing results and a bulk solitary wave, termed a nematicon, can then form [12]. Experiments have been performed demonstrating the practical applications of nematicons [4, 16] for optical transmission and switching [3, 11].

In a thermal medium the refractive index is temperature dependent. Hence, heating by a light beam causes the refractive index to change [8]. Barsi et al. [17] performed experiments on a material whose refractive index decreased with temperature, so that it can support dark, rather than bright, solitary waves. These experiments showed that initial sharp gradients or discontinuities in temperature are smoothed by a dispersive shock wave whose trailing edge consists of dark solitary waves. Similar experiments in a defocusing thermal medium were performed by Conti et al. [18] following theoretical work on both focusing and defocusing thermal media [19]. It has also been found experimentally that, for elliptical and toroidal light beams in a focusing thermal medium, nonlocality results in the elimination of the azimuthal instabilities associated with such an elliptical or toroidal input beam [9]. This nonlocal suppression of instabilities in a toroidal beam also occurs in

a nematic liquid crystal [20, 21].

The evolution of a solitary wave in a nonlocal medium is also affected by the boundaries of the cell. The beam to cell width ratio is a key parameter, see [22, 23]. For a biased nematic liquid crystal cell, for which the molecules are pre-tilted by an external electric field, the response of the molecules decays exponentially away from the beam, so the effect of the boundaries can be ignored in a cell which is wide compared with the beam width [4]. However, for an unbiased cell the response decays linearly in $(1 + 1)$-D and logarithmically in $(2 + 1)$-D, so the effect of the boundaries is important [22, 24]. Alfassi et al. [25] examined solitary wave trajectories in a thermal medium for off-centre initial conditions and non-symmetric boundary conditions, finding good agreement between numerical and observational beam displacement as the boundary temperature difference was varied. Analytical and numerical work applicable to both unbiased liquid crystal cells and thermal media found that the boundaries are repulsive, resulting in an oscillatory solitary wave trajectory before any steady state is achieved [26], in agreement with previous experimental, numerical and theoretical studies [22, 23].

The equations describing solitary wave propagation in nonlinear, nonlocal media usually consist of a coupled NLS-type equation and a Poisson equation for the medium response [4, 8]. Due to the complexity of such a system, no exact solitary wave solutions of these equations have been derived to date. The only solutions which exist are asymptotic solutions in the limit of the nonlocality parameter becoming infinite [27], which is not the experimental limit of interest, as the nonlocality, while large, is not large enough for the infinite limit to be a good approximation. For this reason, approximate and numerical methods for determining solitary wave solutions are of great interest. Much previous work [15, 26, 28] has used modulation theory [29] as an approximate, variational [30], approach, finding good agreement with full numerical solutions [15, 26, 28] and experimental results [31, 32]. Of relevance to the present work, Alberucci et al. [26] examined the boundary induced motion of an optical solitary wave using both numerical and variational based approaches.

Stationary solutions of coupled solitary wave equations can be derived via the substitution of a separable solution that splits the spatial and temporal components. Rasmussen et al. [33] used this technique to investigate the interaction of multiple solitary waves for a range of values of the nonlocality parameter. A recent series of papers by Yang et al. [34, 35, 36] evaluated the stability and performance of numerical schemes for solving NLS-type equations, including the Newton conjugate-gradient method and imaginary time evolution methods. Boyd [37] discusses the challenges of using Newton methods to find solitary wave solutions. Wang [38] explored the use of a split-step finite difference method for solving single and coupled NLS equations in one, two and three dimensions, finding that stable and accurate solutions are obtainable.

In the present work, a system consisting of a coupled NLS-type equation and a Poisson equation which governs nonlocal beam evolution in thermal media is considered. Non-symmetric temperature boundary conditions are applied at the cell boundaries. In §2 the governing equations are described, while in §3 the various iterative numerical schemes used to find solutions of these equations are detailed and their performance for the thermal

media application is benchmarked. The most suitable and efficient method, the Newton conjugate gradient (CG) scheme, is used in §4 to generate results for steady state thermal solitary waves. It is found that the profile and position of the solitary wave in the cell can be easily varied by modifying the temperatures at the cell boundaries. This has implications for optical devices based on such solitary waves [4, 16]. In §5 we consider the stability of the solitary waves both analytically and numerically. Appendix A discusses the choice of stopping condition for the iterative numerical solvers.

2. Governing equations

Let us consider a coherent light beam propagating through a $(1+1)$-D nonlinear, nonlocal medium, such as a thermal medium [5, 6, 8, 9, 10]. Let us impose a coordinate system with the z coordinate in the direction down the cell, with the x coordinate in the direction of polarisation of the light beam, orthogonal to the z direction. In this case, the non-dimensional equations governing the propagation of the beam in the paraxial approximation in $(1+1)$-D are [4, 8]

$$\imath\frac{\partial E}{\partial z}+\frac{1}{2}\frac{\partial^2 E}{\partial x^2}+2E\theta=0, \quad \nu\frac{\partial^2\theta}{\partial x^2}+2|E|^2=0. \tag{1}$$

Here E is the envelope of the slowing varying electric field of the light beam, θ is the temperature of the medium and ν is a parameter measuring the degree of nonlocality. The transverse coordinate x has been non-dimensionalised by the width of the input optical beam, the usual non-dimensionalisation [31], so that the width of the solitary wave is $O(1)$. It is clear that the medium equation, the second of (1), could be solved in terms of a Green's function, leading to a single integro-differential equation for E. However, it is simpler to leave the system in the form (1). The usual experimental regime is the so-called highly nonlocal regime in which ν is large, $\nu=O(100)$ [31]. The specific value $\nu=100$ will then be used in the present work. To investigate the effects of non-symmetric boundary conditions we allow differential heating of the cell boundaries. For the temperature on the right hand cell boundary, a Dirichlet boundary condition is applied, while a mixed boundary condition is applied to the left hand cell boundary. For the electric field the usual Dirichlet boundary conditions are applied at both boundaries. These boundary conditions are

$$E=0, \quad \theta_x-\beta\,(\theta-\theta_B)=0, \quad \text{at} \quad x=-\frac{L}{2}, \quad E=\theta=0, \quad \text{at} \quad x=\frac{L}{2}, \tag{2}$$

where β is the Biot number, L is the non-dimensional width of the cell and θ_B is the ambient temperature at the left hand cell boundary. The mixed condition represents Newton cooling, with $\beta=0$ corresponding to a perfectly insulated boundary and $\beta\to\infty$ to a fixed temperature boundary condition $\theta=\theta_B$.

To find solitary wave solutions of the governing equations (1) and (2) we look for a travelling wave solution of the form $E(x,z)=u(x)e^{i\mu z}$, where u is real. Inserting this form reduces the NLS equation for E and the Poisson equation for θ in (1) to the ordinary differential equations

$$\frac{1}{2}\frac{\partial^2 u}{\partial x^2}+2u\theta-\mu u=0, \quad \nu\frac{\partial^2\theta}{\partial x^2}+2u^2=0, \tag{3}$$

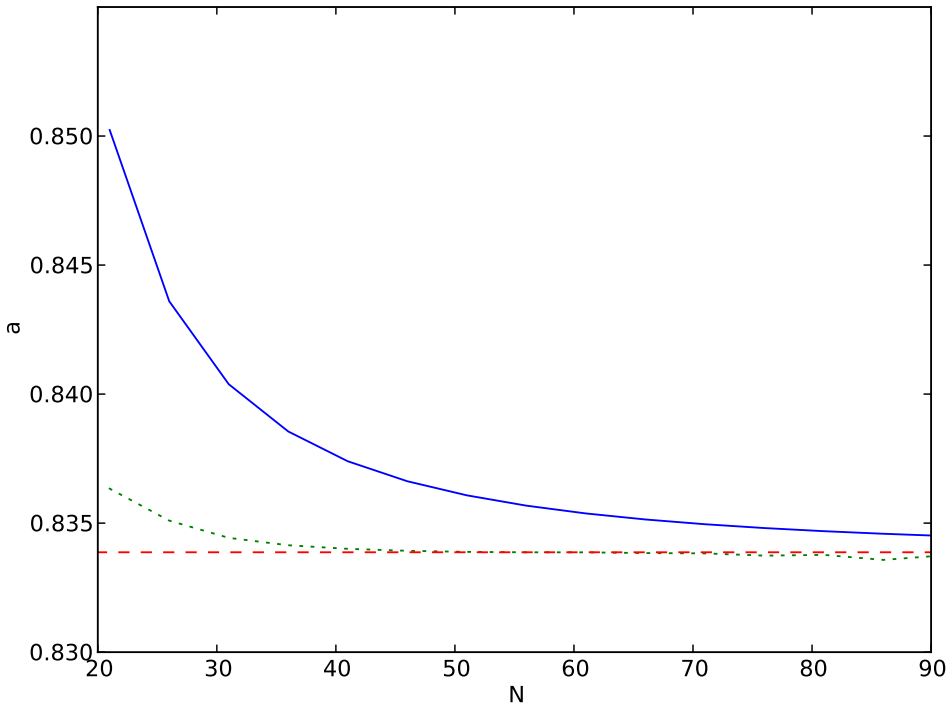

Figure 1. (Colour online) Amplitude of the solitary wave, a, versus the number of grid points N. Shown are results for the second-order discretization (solid line, blue), fourth-order discretization (dotted line, green) and the Richardson extrapolation fifth order estimate for the converged solution (dashed line, red). The other parameters are $\beta = 100$, $\theta_B = 0.2$, $\mu = 1$, $\nu = 100$.

$$u = 0, \quad \theta_x - \beta\,(\theta - \theta_B) = 0, \quad \text{at} \quad x = -\frac{L}{2}, \quad u = \theta = 0, \quad \text{at} \quad x = \frac{L}{2},$$

where the parameter μ is referred to as the propagation constant of the solitary wave.

For the symmetric case, where $\beta \to \infty$ and $\theta_B = 0$, the governing equations (1) and (2) are also applicable to a nematic liquid crystal, see [4, 12, 26], where θ is now the angle of deviation the nematic molecules make with respect to their rest orientation. Hence, there is a close parallel between thermal solitary waves and nematicons. For nematic liquid crystals the system (1) is a good approximation to the full $(2+1)$-D equations governing nonlinear beams in liquid crystals [39] and $\nu = O(100)$ [31].

3. Numerical methods and benchmarking

A variety of different numerical schemes have been used to find steady solitary wave solutions [36]. In this work three of these schemes are implemented and benchmarked to check that consistent solutions are generated and to gauge which is the most efficient for solving the coupled system (1). Considered are the Imaginary Time Evolution Method (ITEM) ([40],[35]), the Accelerated Imaginary Time Evolution (AITE) method ([35]) and the Newton Conjugate Gradient (Newton-CG) method, each following the implementations

used by Yang [36]. One main difference between the implementations used here and in Yang [36] is that we use a direct fourth-order spatial discretization, whereas Yang used a Fourier transform to derive a spectral discretization. Also, the examples considered by Yang did not include the coupled system (1) and (2) of interest here. In the following descriptions of the numerical schemes we consider $v(x)$ where $v = u$ for the ITEM and AITE methods, and $v = (u, \theta)^T$ for the Newton-CG method. All the solvers were iterated until the maximum difference between successive iterations, $\epsilon = ||v_n - v_{n-1}||_2$, reached the stopping condition $\epsilon \leq 10^{-10}$, see Appendix A for details on how this value was chosen. All quoted computation times are based on an Intel Core i5-2500K processor running at 3.3GHz, with programs written in Python 2.6 and NumPy 1.6.1.

3.1. Description of iterative methods

To implement the ITEM and AITE methods, equation (3) for a steady solitary wave is written in the form

$$L_{00}v(x) = \mu v(x), \text{ where } L_{00} \equiv \frac{1}{2}\frac{\partial^2}{\partial x^2} + 2\theta. \tag{4}$$

In the discussion below, L, L_0, L_{00} and M are all operators, which correspond to matrices once a finite difference approximation for $\frac{\partial^2}{\partial x^2}$ is applied. For the ITEM method we consider the equation $v_t = L_{00}v$ obtained by replacing z with $-it$. This equation is numerically integrated using the Euler method. At each iteration v_n the solution must be normalized to a fixed power to prevent the solution from diverging to infinity or decaying to zero. The ITEM iterative method can be written as

$$v_n^* = \frac{P}{< v_n, v_n >} v_n, \quad v_n = (1 + L_{00}\Delta t)v_{n-1}^*, \quad < u, v >= \int_{L/2}^{L/2} uv dx, \tag{5}$$

where P is the fixed power of the converged solitary wave and Δt is the size of the discretization step. Note that Δt is not a time step. The system (5) is iterated until the solution converges. The AITE method iterates the equation $v_t = M^{-1}(L_{00}v - \mu v)$ where M is a a preconditioning matrix to improve the rate of convergence of the scheme, by modifying its condition number. We choose $M = c - \partial^2/\partial x^2$ with $c = 1.5$ as the preconditioning matrix. The threshold value of the disctretization step Δt at which instability begins to occur for the AITE and ITEM schemes depends on the eigenvalues of the operator

$$L\Psi = M^{-1}\left(L_1\Psi - \frac{\langle L_1\Psi, M^{-1}v\rangle}{\langle v, M^{-1}v\rangle}v\right), \tag{6}$$

where L_1 is the linearisation operator of Lv wrt to v. Yang [35] derived the relation $\Delta t_{max} = -2/\Lambda_{min}$, where Λ_{min} is the minimum eigenvalue of the operator L, to give the maximum value of Δt for which the imaginary time method converges.

To implement the Newton-CG method, we consider (4) in the form $L_0v(x) = 0$, where $L_0 = L_{00} - \mu$. Given an approximate solution v_n, we can write $v = v_n + e_n$, where v is the exact solution and e_n is the error. Substituting this into (4) and neglecting higher-order terms in e, we obtain

$$L_{1n}\Delta v_n = -L_0 v_n, \tag{7}$$

Method	Number of Grid Points	Computation Time (secs)
Second Order	106	31.3
Fourth Order	36	2.9

Table 1. Number of discretization grid points and amount of computation time required to converge to stopping condition $\epsilon \leq 1 \times 10^{-10}$

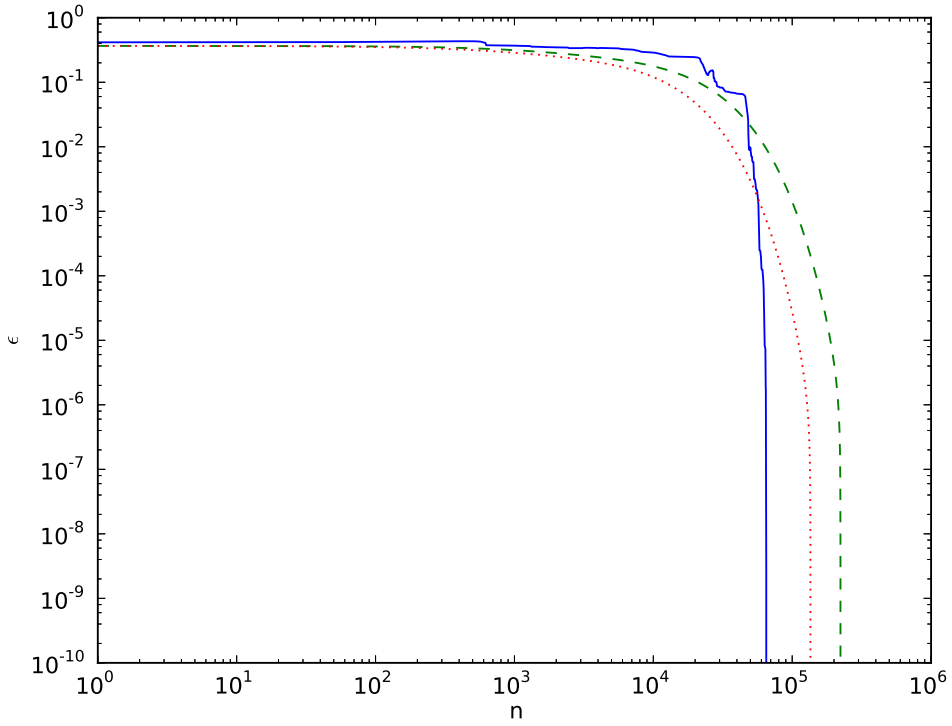

Figure 2. (Colour online) Comparison of convergence rates for the numerical schemes, with the maximum error between each iteration and the numerical solution, ϵ, versus the number of iterations, n. Shown are the results for the Newton-CG method (solid line, blue), AITE method (dotted line, green) and ITEM method (dashed line, red).

where the next approximation is $v_{n+1} = v_n + \Delta v_n$ and L_{1n} is the linearisation operator evaluated at the iterate v_n. Equation (7) is solved for Δv_n using the conjugate gradient method. In general, the convergence of the conjugate gradient method requires that the matrix L_{1n} be self-adjoint, which is not the case here. To circumvent this, we pre-multiply both sides of (7) by L_{1n}^T prior to solving. This has the effect of greatly increasing the condition number of the matrix $(L_{1n}^T L_{1n})$ and also the computation time, but does not change the solution, and ensures that the method converges.

One drawback of the AITE and ITEM methods is that they do not converge to the correct solution if the method is implemented to solve for a single solution vector $v = (u, \theta)^T$. To successfully implement these methods, the numerical scheme was then applied to the NLS-type equation only (where $v = u$) and after each iteration a number of Gauss-Seidel iterations of the Poisson equation were applied to solve for θ.

Method	Iterations	Computation Time (mins)
ITEM	135316	3.89
AITE	222643	9.15
Newton-CG	65049	0.09

Table 2. Number of iterations and computation time required to reach stopping condition $\epsilon =\leq \times 10^{-10}$ for the three numerical schemes.

Method	Iterations	Computation Time (seconds)
No Preconditioning	68490	13.5
Diagonal Elements of L_1	44672	13.0
Diagonal Scale Matrix	55517	9.4
Diagonal Elements of $L_1 - \theta$	45674	12.4

Table 3. Number of iterations and computation times required for the Newton-CG method to reach the stopping condition $\epsilon \leq 1 \times 10^{-10}$ for a number of different preconditioning matrices.

3.2. Order of the spatial discretization

The performances of the second and fourth-order finite difference implementations of the Newton-CG will now be compared. To implement the fourth-order scheme a non-symmetric finite difference stencil was used for the second of (3) at the first interior point and for the boundary condition,

$$\begin{aligned} &48\theta_1 - 3\theta_4 + 16\theta_3 - 36\theta_2 - 25\theta_0 - 12\beta\Delta x(\theta_0 - \theta_B) = 0, \\ &\theta_0 - 15\theta_1 - 4\theta_2 + 14\theta_3 - 6\theta_4 + \theta_5 + 24\Delta x^2|u_1|^2 = 0. \end{aligned} \tag{8}$$

Figure 1 shows the solitary wave amplitude, a, versus N, the number of grid points. The other parameters are $\beta = 100$, $\theta_B = 0.2$, $\mu = 1$ and $\nu = 100$. Both the second and fourth-order implementations asymptotically approach the exact solution as the number of discretization points is increased. Also shown in Figure 1 is a fifth order approximation to the exact solitary wave amplitude derived using Richardson extrapolation. Appendix A discusses the Richardson extrapolation procedure.

Table 1 shows the number of grid points and computation time needed to achieve a fixed accuracy. The parameters considered are those used in Figure 1 and the chosen accuracy for the solitary wave amplitude a is an error of less than 1×10^{-4}. It can be seen that the fourth-order method requires far fewer grid points to obtain the same accuracy as the second order method. Due to the reduction in grid points the fourth-order method is an order of magnitude faster than the second-order method. This increased efficiency, while useful for the $(1+1)$-D geometry, is of vital importance for a future implementation of the method in $(2+1)$-D.

3.3. Convergence rates

To check the convergence rates it is first necessary to make sure the methods are converging to the same solution, as a solitary wave is a one parameter solution. The propagation constant μ can be chosen as this parameter. One of the differences between the imaginary time and the Newton-CG methods is that in the imaginary time method the power of the solitary wave is scaled to a fixed value to ensure that the numerical scheme does not diverge, so that a solution for a pre-determined value of μ is not found, but the method chooses its own value of μ. In contrast, the Newton-CG method the solution power is controlled by the propagation constant μ. The power of the solitary wave

$$P = \int_{-L/2}^{L/2} |u|^2 \, dx, \tag{9}$$

found using the Newton-CG method is $P = 3.246$ for the case $\mu = 1$. When this value of the power is used to scale the AITE and ITEM methods, the three iterative methods converge to the same solution.

Figure 2 shows the number of iterations versus the difference between successive iterations, ϵ, for the three iterative solvers. Shown are the results for the ITEM, AITE and Newton-CG methods. The parameters are $\theta_B = 0.2$, $\nu = 100$, $\mu = 1$, $\beta = 100$, $\Delta x = 0.33$ and $\Delta z = 0.003$. Table 2 shows the number of iterations and computation times, for convergence with $\epsilon < 10^{-10}$, for the examples of Figure 2. The curve for the Newton-CG method shows both the Newton and CG iterations. For the ITEM and AITE methods ϵ decreases smoothly, whilst it does not for the Newton-CG method. However, the figure and table show that the Newton-CG method is several orders of magnitude faster than the other methods, due to the lower number of total iterations and the lower computational cost of the conjugate gradient iterations. For the Newton-CG method the total number of iterations is comprised of 294 Newton iterations, with, on average, 221 conjugate gradient steps for each Newton iteration. The error estimates for the conjugate gradient iterations within a given Newton step decrease smoothly, but the error estimate can increase between Newton iterations. Also note that the AITE method is actually slower than the ITEM, because the performance gain due to preconditioning does not offset the extra computational overhead associated with this method.

We then conclude that the Newton-CG method is clearly the most natural and efficient choice for finding the steady solitary wave solution of (3), due to its ability to solve the coupled equations for u and θ in a unified manner, and its faster (a factor of over 100 times) convergence time.

3.4. Preconditioning

To increase the speed of convergence of the Newton-CG method a number of different preconditioning matrices M^{-1} for the numerical scheme (7) were used. The computation speeds for the different choices of matrices are shown in Table 3. All of the preconditioning matrices yielded only slight performance gains, if any. The most beneficial of those tested was the matrix for which M contains the diagonal elements of L_0. However, the

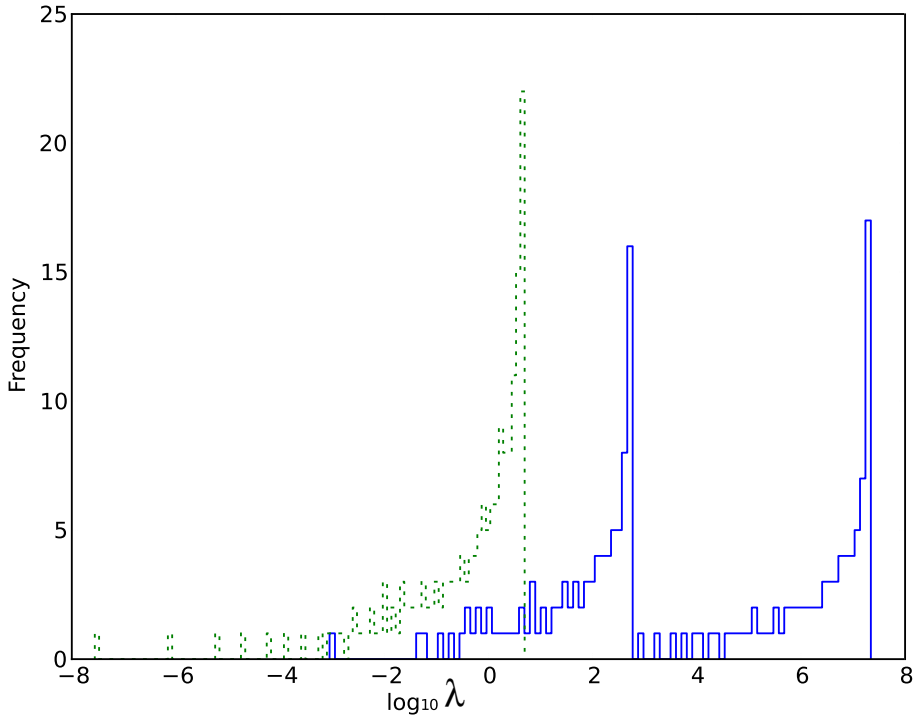

Figure 3. (Colour online) Conjugate gradient scheme eigenvalue distributions for no preconditioning (solid line, blue) versus preconditioning matrix containing diagonal elements of L_1 (dotted line, green).

performance increase was slight. When the preconditioning matrix and pre-multiplication by the transpose are both applied, the numerical scheme (7) becomes

$$(M^{-1}L_1)^T M^{-1}L_1 v_{1n} = -(M^{-1}L_1)^T M^{-1} v_n. \tag{10}$$

Figure 3 shows the distribution of eigenvalues for the numerical scheme. Note that the set of eigenvalues changes with each iteration, but approaches a fixed set of values as the numerical method converges and the changes in L_0 and L_1 become small. The figure shows the eigenvalue distribution for the iterations immediately prior to convergence. For the case with no pre-conditioning there are two clusters of eigenvalues, with peaks in the distribution around $\lambda = 2 \times 10^7$ and 5.5×10^2, and a condition number of $\kappa = 2.5 \times 10^{10}$. For the pre-conditioned case there is a single cluster of eigenvalues, with a peak in the distribution around $\lambda = 4.5$ and a lower condition number of $\kappa = 1.8 \times 10^8$. The coupled nature of the equations means that in the non-preconditioned version of the scheme, corresponding to $M = I$, there is a bimodal distribution of eigenvalues and a large condition number. Once the diagonal pre-conditioner has been applied the bimodal distribution is eliminated and there is a much smaller condition number, with corresponding performance gains for the numerical scheme.

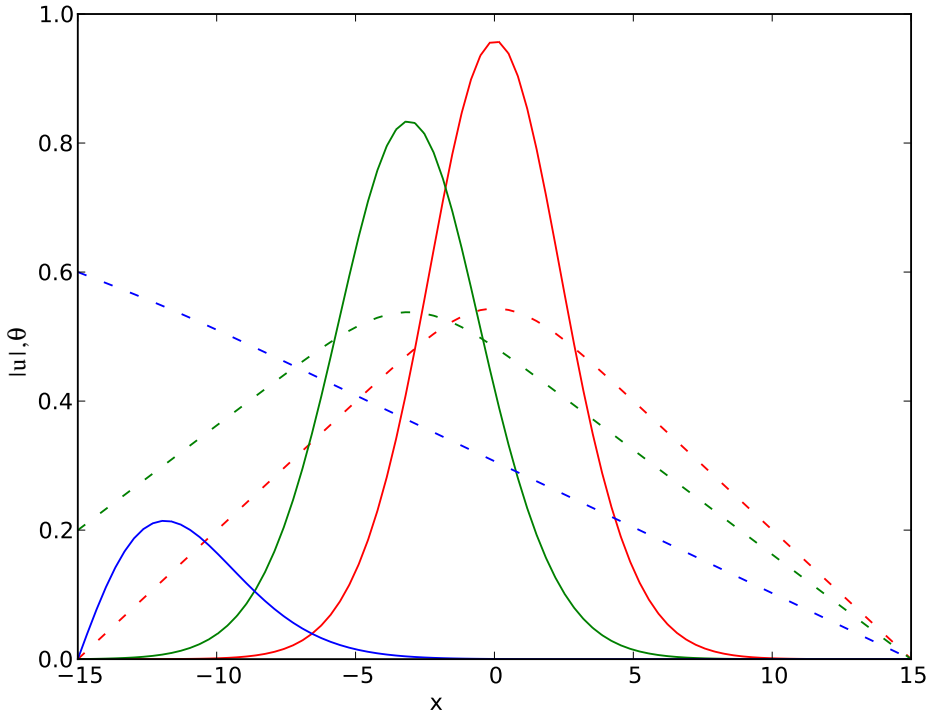

Figure 4. (Colour online) Thermal solitary waves, large β case. Shown are the electric field, $|u|$ (solid), and temperature, θ (dashed), versus x. The three solitary waves are $\theta_B = 0$ (red, center), $\theta_B = 0.2$ (green, slightly offset) and $\theta_B = 0.6$ (blue, near boundary). The other parameters are $\beta = 100$, $\nu = 100$ and $\mu = 1$. The peak of the $\theta_B = 0$ wave is located at $x = 0$, the other waves move towards the left-hand boundary for non-zero θ_B.

4. Results and discussion

In the previous section it was shown that the Newton-CG technique is the most efficient and versatile iterative method for finding solitary wave solutions of the coupled system (1) and (2). In this section the Newton-CG method shall be used to explore the solution space for our coupled system and the effects of non-symmetric temperature boundary conditions for the cell. In all the examples considered here we use a cell of length $L = 30$ and choose $\Delta x = 0.33$.

Figure 4 shows thermal solitary wave solutions of (1) and (2) for large heat loss β. Shown are the electric field, $|u|$, and temperature, θ, versus x. The three solitary waves are for $\theta_B = 0$, 0.2 and 0.6. The other parameters are $\beta = 100$, $\nu = 100$ and $\mu = 1$. When $\theta_B = 0$ both cell boundaries are at the same temperature and the solitary wave is symmetric, with the peak of the solitary wave, of amplitude $a = 0.96$, located at the centre of the cell, $x = 0$. In this case the thermal solitary waves are equivalent to nematic solitary waves in a finite cell, described in [26]. As the ambient temperature, θ_B, of the left-hand cell boundary increases, the peak of the solitary wave decreases in amplitude and moves towards the warmer boundary, as found in [25]. For the $\theta_B = 0.2$ case the peak

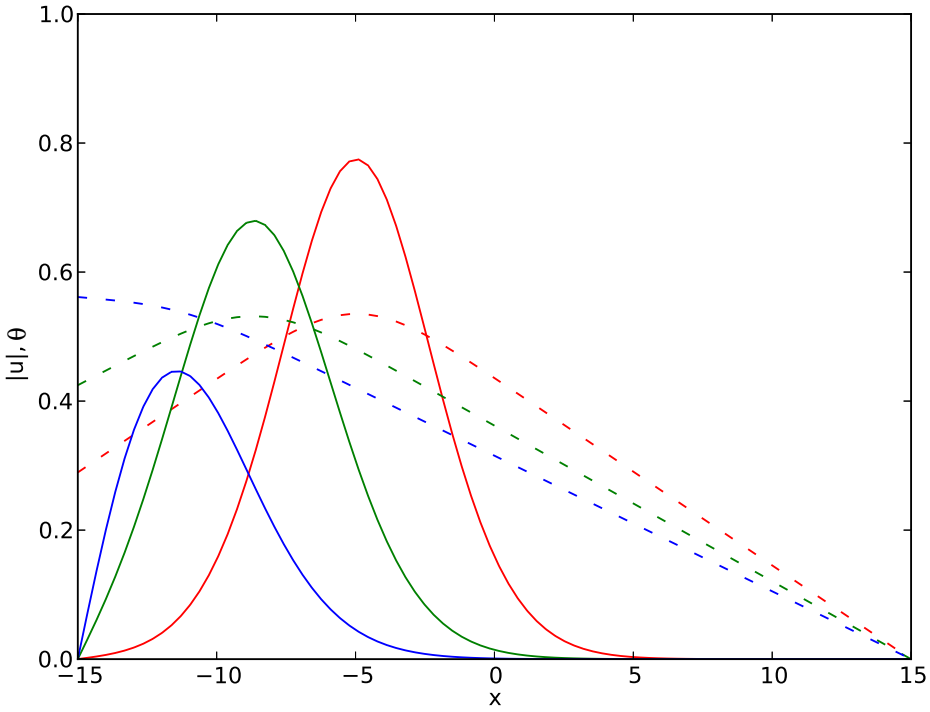

Figure 5. (Colour online) Thermal solitary waves, small β case. Shown are the electric field, $|u|$ (solid), and temperature, θ (dashed), versus x. The three solitary waves are $\theta_B = 0$ (red, nearest to center), $\theta_B = 0.2$ (green) and $\theta_B = 0.6$ (blue, nearest to boundary). The other parameters are $\beta = 0.1$, $\nu = 100$ and $\mu = 1$. The peak of the $\theta_B = 0$ wave is located at $x = -5.1$, the other waves move toward the left-hand boundary for non-zero θ_B.

amplitude has decreased to $a = 0.83$ and is located at $x = -3.2$. For $\theta_B = 0.6$ the wave is located at $x = -11.9$, close to the cell boundary, and the amplitude is much reduced, to $a = 0.215$. In this case the temperature profile is a near linear variation between the two ambient values of $\theta = 0.6$ and 0. For small values of θ_B the peak values of $|u|$ and θ are co-located. However, as θ_B becomes large this is no longer the case and the peak θ value is found closer to the edge of the cell. It may also be noted that for small θ_B the slope of the temperature profile near the left cell boundary is positive, whereas for the large θ_B case this slope is negative. For the small θ_B examples the electric field amplitude is large and the pulse causes significant internal heating of the medium. The positive temperature profile at the left hand cell boundary indicates that some of this generated heat is being lost at the cell boundary. For the $\theta_B = 0.6$ case, however, little internal heat generation occurs, as the electric field amplitude is small, and the negative slope of the temperature profile indicates the cell is being heated via the warmer cell boundary.

Figure 5 shows thermal solitary wave solutions of (1) and (2) for low heat loss β. Shown are the electric field, $|u|$, and temperature, θ, versus x. The three solitary waves are for $\theta_B = 0$, 0.2 and 0.6. The other parameters are $\beta = 0.1$, $\nu = 100$ and $\mu = 1$. For this

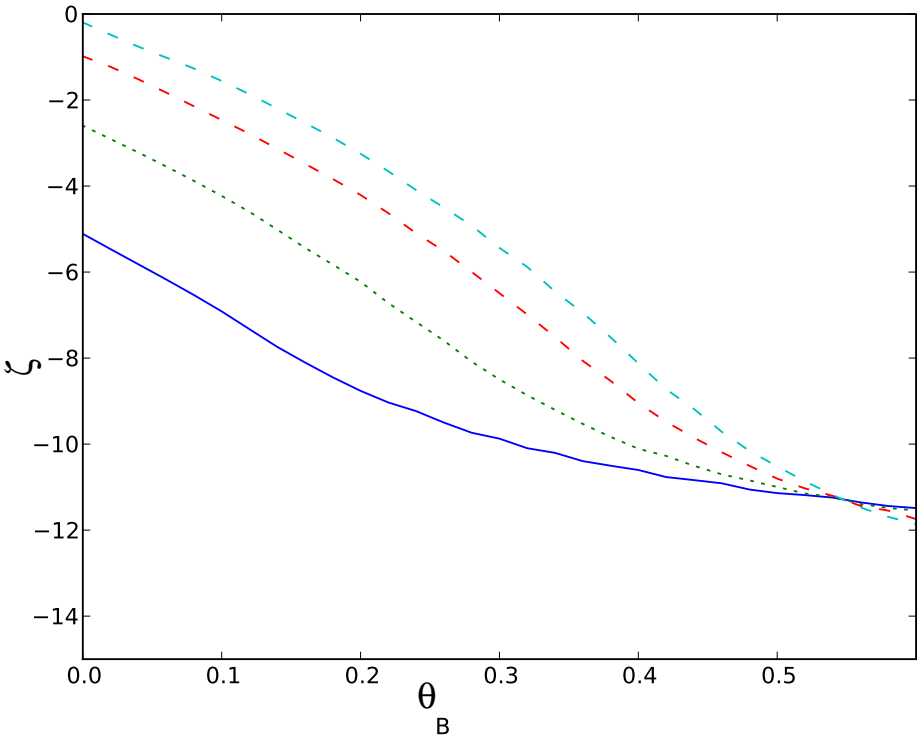

Figure 6. (Colour online) Location of the peak of thermal solitary wave, ζ, versus the ambient temperature, θ_B, for $\mu = 1$. The curves correspond to $\beta = 0.1$ (solid line, dark blue), $\beta = 0.2$ (dotted line, green), $\beta = 0.6$ (lower dashed line, red) and $\beta = 10$ (upper dashed line, light blue).The edge of the domain is at $x = -\frac{L}{2} = -15$.

figure the parameters are the same as for Figure 4, except for the Biot number, which is small. In this case, when $\theta_B = 0$ the steady-state temperature at the left cell boundary is $\theta(-L/2) = 0.29$ and the peak of the solitary wave, of amplitude $a = 0.77$, which is located at $x = -5.1$. This wave shows some qualitative and quantitative differences compared with the $\theta_B = 0$ wave for the large β example of Figure 4. The wave is non-symmetric, being located closer to the left hand cell boundary, and its amplitude is lower. As θ_B increases, the steady state temperature at the left cell boundary increases and approaches θ_B. As for the large β case, the waves migrate towards the left hand cell boundary as this edge of the cell heats up. For the $\theta_B = 0.2$ case the peak amplitude has decreased to $a = 0.68$ and is located at $x = -8.75$. For $\theta_B = 0.6$, the amplitude of the solitary wave is further reduced, to $a = 0.45$ and the solitary wave peak is now located much closer to the cell boundary, at $x = -11.5$. The temperature at the left cell boundary is $\theta(-L/2) = 0.56$, close to the ambient value and the temperature profile is near linear, with negative slope, for the same reason as the equivalent large β case. Again, as in the large β case, the $|u|$ and θ maxima are co-located for small θ_B, and the temperature maximum is close to the edge of the cell for large θ_B.

Figure 6 shows the location of the peak of thermal solitary wave, ζ, versus the ambient temperature, θ_B, for $\mu = 1$. The curves correspond to $\beta = 0.1$, 0.2, 0.6 and 10. The $\beta = 10$

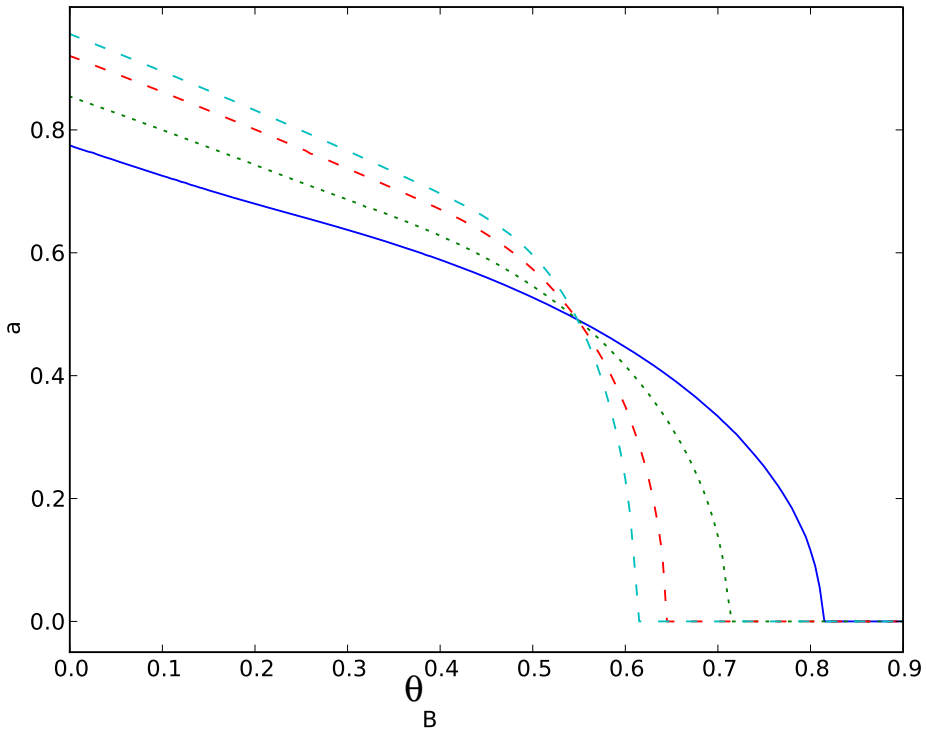

Figure 7. (Colour online) Amplitude of the thermal solitary wave, a, versus the ambient temperature, θ_B, for $\mu = 1$. The curves correspond to $\beta = 0.1$ (solid line, dark blue), $\beta = 0.2$ (dotted line, green), $\beta = 0.6$ (lower dashed line, red) and $\beta = 10$ (upper dashed line, light blue). The $\beta = 10$ curve is above the $\beta = 0.6$ curve, on the left hand side.

curve is very close to the result obtained in the large Biot number limit $\beta \to \infty$. As the ambient temperature at the left hand cell boundary is increased, the thermal solitary wave migrates towards the left hand edge of the cell. Once θ_B exceeds 0.6, the numerical scheme converges to $u = 0$. Hence, no thermal solitary waves exist once the difference in ambient temperatures between the two sides of the cell is greater than a certain limit. Physically, this is due to the fact that the solitary wave breaks down once it is pushed too close to the cell wall. Increasing the Biot number, β, also causes the solitary wave to shift towards the left hand cell boundary.

Figure 7 shows the amplitude of the thermal solitary wave, a, versus the ambient temperature, θ_B, for $\mu = 1$. The curves correspond to $\beta = 0.1$, 1, 10 and 100. For a given choice of β, the solitary wave amplitude decreases as θ_B increases. The solitary wave amplitude decreases to $a \approx 0$ at a given value of θ_B, after which thermal solitary waves do not exist. This threshold value of θ_B decreases as β increases from $\theta_B = 0.82$ at $\beta = 0.1$, to $\theta_B = 0.6$ at $\beta = 100$.

Figures 8(a) and (b) show the thermal solitary wave amplitude, a and location, ζ, respectively, in the (θ_B, β) parameter space for $\mu = 1$. Note that, as expected, increasing θ_B causes the amplitude of the solitary wave to decrease, as well causing it to migrate towards the left hand edge of the cell. For the range of Biot number $0 \leq \beta \leq 1.2$ shown

in the figure, the solitary wave amplitude is non-zero for $0 \leq \theta_B \leq 0.6$. As β increases, the solitary wave amplitude decreases and approaches a constant value for a given θ_B. In addition, the solitary wave position migrates towards the left hand cell boundary with decreasing Biot number β.

The Newton C-G method can also be used to solve for excited state thermal solitary waves. This ability is another advantage of the Newton-CG method, as the imaginary time methods do not converge to these excited state solutions. Figure 9 shows excited state thermal solitary wave solutions of (1) and (2). Shown are the electric field, $|u|$, and temperature, θ, versus x. The three solitary wave solutions are for $\theta_B = 0$, 0.1 and 0.2. The other parameters are $\beta = 100$, $\nu = 100$ and $\mu = 0.2$. This figure shows that the electric field amplitude $|E|$ has three peaks, so that the waves correspond to the first excited state. In contrast, the temperature response θ has a single peak. This is due to heat diffusion, which smooths out the temperature response for large ν. For $\theta_B = 0$ the solitary wave is symmetric, with a peak of amplitude $a = 0.36$ located at $x = 0$ and a peak of amplitude $a = 4.01$ located at $x = \pm 5.3$. This example is equivalent to the (symmetric) first excited state nematicon in a nematic liquid crystal [41]. For the case $\theta_B = 0.1$ the peaks have shifted towards the left hand cell boundary and decreased in amplitude, with peaks of $a = 0.316$ at $x = 4.1$, $a = 0.28$ at $x = -3.4$, and $a = 0.3$ at $x = -10.9$. For the $\theta_B = 0.2$ the temperature profile is now nearly linear and the peak amplitudes are $a = 0.18$ at $x = 0.54$, $a = 0.15$ at $x = -6.9$, and $a = 0.135$ at $x = -13.7$. Beyond this, for $\theta_B > 0.24$, the excited state solitary waves do not exist. Excited state thermal solitary waves exist for a smaller range of ambient temperature θ_B than do the ground state waves, as they break down faster as the left most peak approaches the left hand boundary.

5. Stability of the solitary waves

The stability of the thermal solitary waves is now investigated, both analytically and numerically. Power versus propagation constant curves are calculated for the families of thermal solitary waves corresponding to (3). The optical power (9) is calculated using the numerical solitary waves found using the Newton-CG method. Solitary wave solutions of generalised NLS equations on an infinite domain are modulationally stable in regions of parameter space for which the power versus propagation constant curve has positive slope ($dP/d\mu > 0$), see, for example, [42, 43, 44]. This result has not been theoretically proven for the governing equations (1) and (2), which is a NLS-type system on a finite domain, but the results presented here are consistent with the theory for the NLS equation on an infinite domain.

These analytical stability predictions are compared with the results of numerical simulations of the original governing pdes (1) and (2), using the numerical steady state solution as an initial condition. The initial condition used is

$$E(x,0) = u_s(x) + \epsilon_0 \cos(0.2x), \quad \theta(x,0) = \theta_s(x), \tag{11}$$

where $u_s(x)$ and $\theta_s(x)$ is the thermal solitary wave solution found using the Newton-CG method. For the examples considered below, ϵ_0 is taken as 0.5% of the amplitude of the

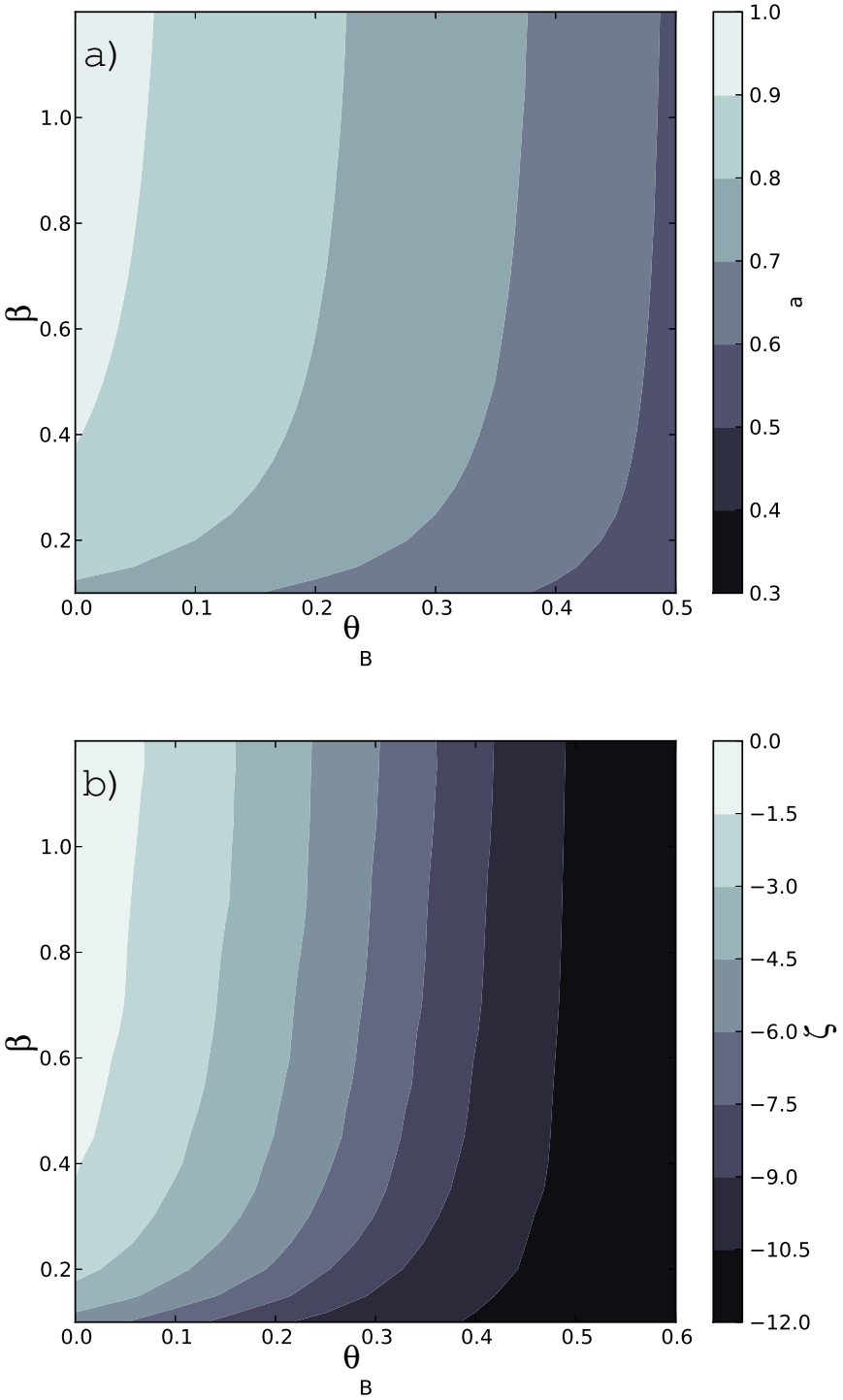

Figure 8. (Colour online) Thermal solitary wave (a) amplitude a and (b) position ζ in the (θ_B, β) parameter space for $\mu = 1$. The edge of the domain is at $x = -\frac{L}{2} = -15$.

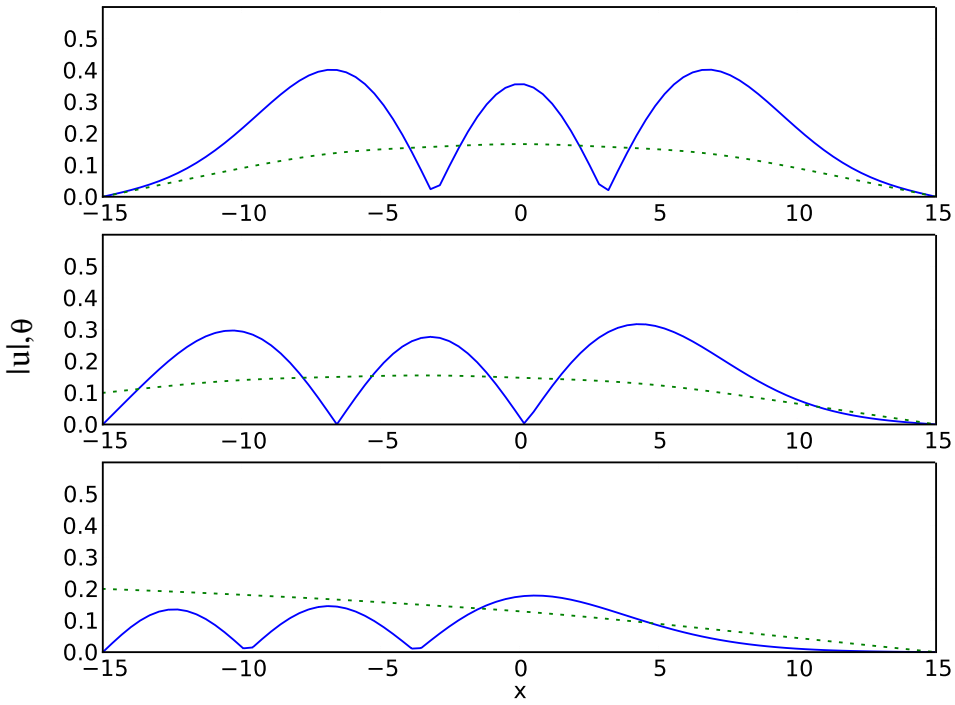

Figure 9. (Colour online) Excited state thermal solitary waves. Shown are the electric field, $|u|$ (blue, solid lines), and temperature, θ (green, dotted lines), versus x. The three solitary waves are $\theta_B = 0$ (top panel), $\theta_B = 0.1$ (middle) and $\theta_B = 0.2$ (bottom). The other parameters are $\beta = 100$, $\nu = 100$ and $\mu = 0.2$.

solitary wave. The numerical solution of the electric field equation is obtained using a hybrid numerical method, for which the spatial derivatives are discretized using central finite differences and the fourth order Runge-Kutta method is used to advance in the time like variable z. Gauss-Seidel iteration used to solve for the temperature at each z-step [45]. The spatial discretizations used are $\Delta z = 0.03$ and $\Delta x = 0.33$.

Figure 10 shows the power P versus propagation constant μ for ground state thermal solitary waves. The parameters are $\beta = 100$ and $\nu = 100$. The three curves correspond to $\theta_B = 0$, 0.2 and 0.4. For non-zero ambient temperature θ_B the solitary wave solution branch only exists over a finite range of μ. All three curves are monotonic with positive slope indicating that, for a given value of the ambient temperature, there is a single stable solution branch. Figure 11 shows the power P versus propagation constant μ for ground and excited state thermal solitary waves. The parameters are $\theta_B = 0.2$, $\beta = 100$ and $\nu = 100$. The three curves correspond to the ground state and the first two excited states. In all three cases the curves are monotonic with positive slope, indicating modulational stability across the entire range of μ values for both the ground and excited state solitary waves. Hence, it is predicted that the thermal solitary waves are stable for all possible parameter values.

Figure 12 shows the electric field, $|E|$, and temperature, θ, in the (x, z) plane, and

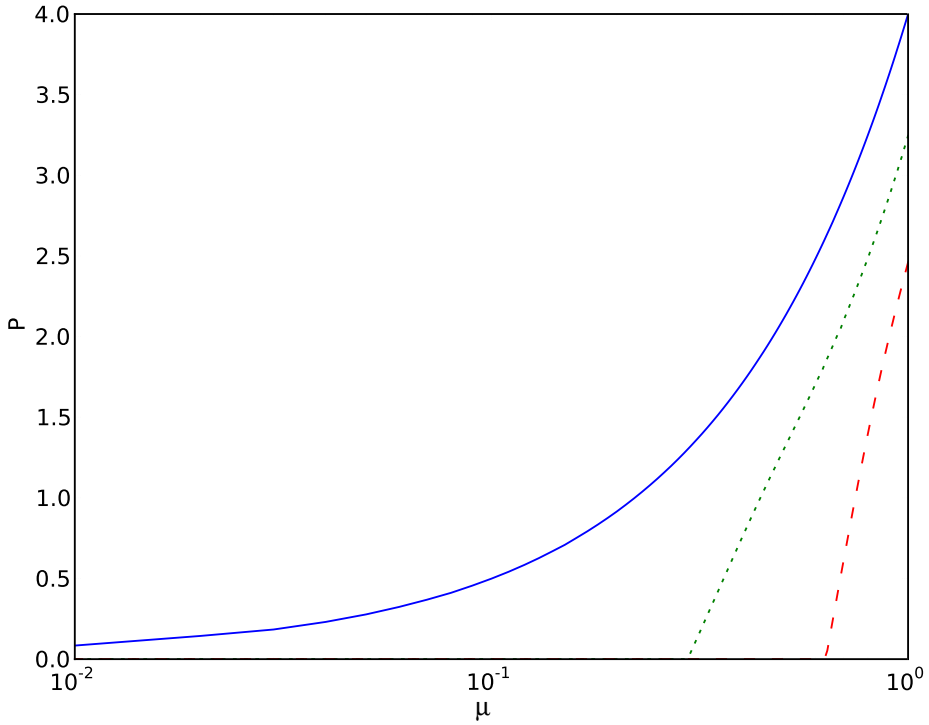

Figure 10. (Colour online) Power, P, versus propagation constant μ, for ground state thermal solitary waves. The parameters are $\beta = 100$ and $\nu = 100$. Curves are $\theta_B = 0$ (blue, solid line), $\theta_B = 0.2$ (green, dotted line) and $\theta_B = 0.4$ (red, dashed line).

the maximum values of $|E|$ and θ, versus z, as given by the full numerical solution of (1) and (2). Shown is the numerical evolution of a perturbed solitary wave, for z up to 10000. The parameters are $\theta_B = 0.2$, $\mu = 1$, $\nu = 100$ and $\beta = 100$. The initial thermal solitary wave corresponds to a non-symmetric case in Figure 4. In this case the thermal solitary wave is a ground state beam centred on $x = -3.19$ with an amplitude of $a = 0.833$. The positions of the peaks of the electric field $|E|$ and temperature θ both remain steady out to $z = 10000$. The electric field amplitude oscillates between $|E| = 0.828$ and $|E| = 0.844$. The oscillations in temperature are much lower, due to diffusive effects.

Figure 13 shows the electric field, $|E|$, and temperature, θ, in the (x, z) plane, and the maximum value of $|E|$, versus z. Shown is the numerical evolution of a perturbed solitary wave for z up to 10000. The parameters are $\theta_B = 0.6$, $\mu = 1$, $\nu = 100$ and $\beta = 100$. The initial thermal solitary wave corresponds to the highly non-symmetric case in Figure 4. In this example the thermal solitary wave is a ground state beam centred at $x = -11.87$, which is very close to the cell boundary at $x = -L/2 = -15$. In this case, the electric field peak amplitude is $a = 0.217$, which is much lower than the example considered in Figure 12 for which the solitary wave peak is near the centre of the cell. This is a more challenging example as the position offset is large and the solitary wave is qualitatively quite different to near symmetric solitary waves or those in an infinite domain. There is a

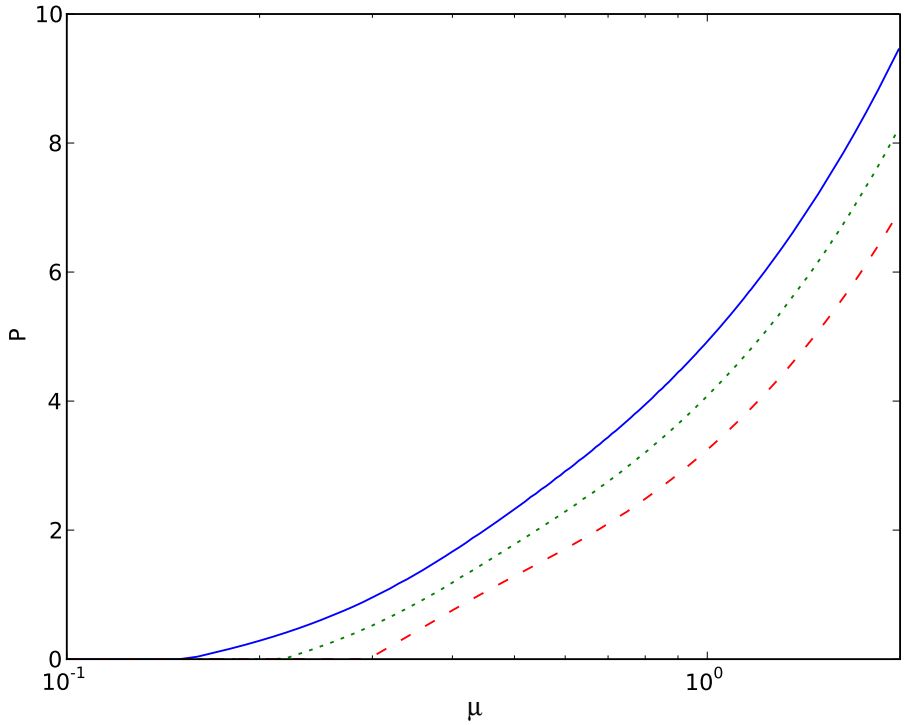

Figure 11. (Colour online) Power, P, versus propagation constant, μ, for ground and excited state thermal solitary waves with $\theta_B = 0.2$, $\beta = 100$ and $\nu = 100$. Shown are the ground state wave (red, dashed line), first excited state (green, dotted line) and second excited state (blue, solid line).

variation in $|E|$ of 2.07% about the mean, which is higher than for the previous example. The temperature does not vary, as it is close to the cell boundary, so it is not shown.

Figure 14 shows the electric field, $|E|$, and temperature, θ, in the (x, z) plane and the maximum value of $|E|$, versus z. Shown is the numerical evolution for a perturbed solitary wave for z up to 10000. The parameters are $\theta_B = 0.2$, $\mu = 0.28$, $\nu = 100$ and $\beta = 100$. The initial thermal solitary wave corresponds to a non-symmetric excited state. For this example, the electric field has two peaks, one of $|E| = 0.222$ at $x = -4.36$ and the other peak of $|E| = 0.187$ nearer to the boundary at $x = -11.76$. It is of interest to determine whether higher order thermal solitary waves are numerically stable, as higher order solitary waves tend to be unstable, particularly for local equations [3]. The maximum value reached for the larger peak is $|E| = 0.224$, with a variation of around 1.1%, which indicates that it is stable to perturbations. As in the previous figure, the maximum temperature does not vary.

Note that although the evolution is shown in all these figures up to $z = 10000$, the initial conditions used were found to be stable for much longer z. Hence, the numerical results confirm that thermal solitary waves are modulationally stable, even for higher-order waves and extremely non-symmetric cases, for which the wave is close to one cell boundary.

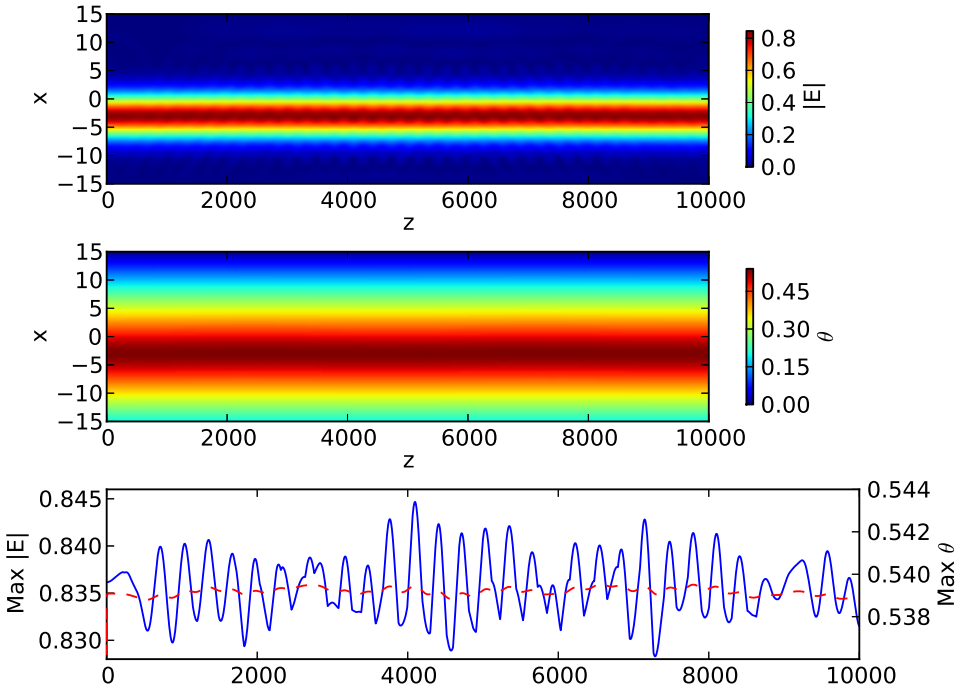

Figure 12. (Colour online) Numerical solutions of (1) and (2). Shown are the electric field amplitude $|E|$ and temperature θ in the (x, z) plane, and the maximum values of $|E|$ and θ, versus z, up to $z = 10000$. The parameters are $\mu = 1.0$, $\theta_B = 0.2$, $\beta = 100$ and $\nu = 100$. Upper panel: $|E|$. Middle panel: θ. Lower panel: Maximum value of $|E|$ (solid line, blue) and θ (dashed line, red).

The power versus propagation constant curves also suggest a theoretical confirmation of solitary wave stability, even though the theoretical result is only valid for NLS waves on an infinite domain.

Section 4 presents thermal solitary wave solutions found by the Newton-CG method. These results suggest that a critical θ_B value exists beyond which no thermal solitary wave exists, as it forms too close to the cell boundary. Some numerical simulations of the original governing pdes (1) and (2) were performed to test the idea that a critical θ_B exists. The thermal solitary wave solutions presented in figures 4 (large β) and 5 (small β) with $\theta_B = 0.6$ represent solutions with peaks close to the left hand cell boundary. These solutions were used as initial conditions for numerical simulations of the governing pdes, but with a slightly larger value of $\theta_B > 0.6$ chosen. These initial conditions evolved to $|E| = 0$ at large z, providing additional evidence that thermal solitary waves do not exist for θ_B beyond a critical value.

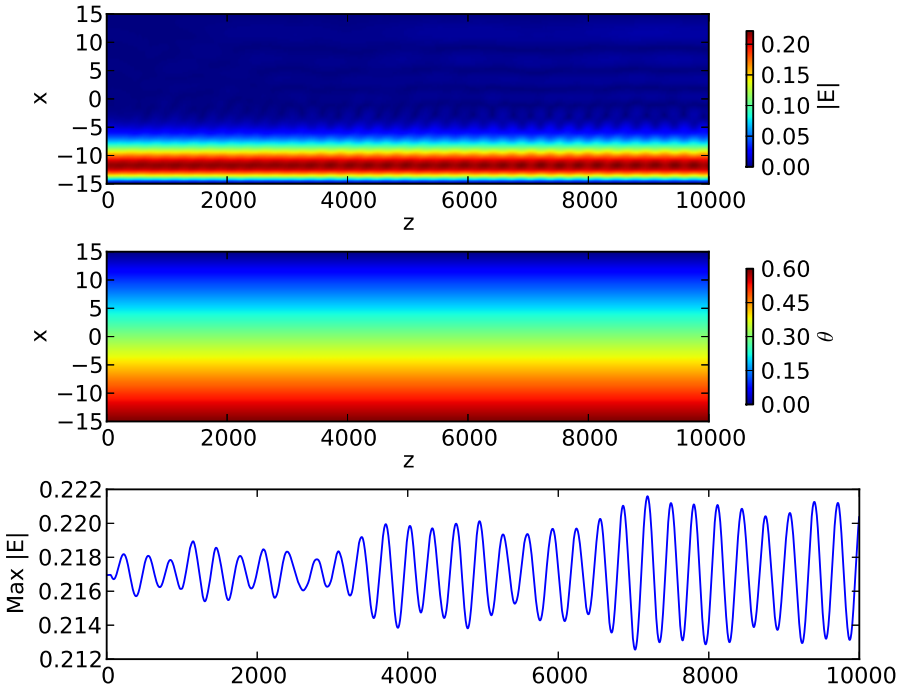

Figure 13. (Colour online) Numerical solutions of (1) and (2). Shown are the electric field $|E|$ and temperature θ in the (x, z) plane, and the maximum value of $|E|$, versus z, up to $z = 10000$. The parameters are $\mu = 1.0$, $\theta_B = 0.6$, $\beta = 100$ and $\nu = 100$. Upper panel: $|E|$. Middle panel: θ. Lower panel: maximum value of $|E|$ (solid line, blue).

6. Conclusions and future work

We have demonstrated that a number of numerical schemes are able to find solitary wave solutions of a coupled system of equations describing beam evolution in a nonlinear, nonlocal thermal media. Of the numerical methods considered, the Newton-CG method is the most suitable, having more rapid convergence and the ability to find excited state thermal solitary waves. It was shown both analytically and numerically that the thermal solitary waves are stable, including the excited states. The solutions derived here show that the location of an optical beam within a cell migrates towards the warmer boundary, which may have applications for the control and steering of light beams in photonic devices. The rapid convergence of the Newton-CG method shows that it has great promise as a suitable method for finding numerical solutions for $(2 + 1)$-D thermal solitary waves governed by the obvious extension of the system considered here. While $(1 + 1)$-D solitary waves can be generated in nonlocal, nonlinear media using cylindrical lenses, in most experiments and applications such solitary waves have a fully two dimensional profile. In future work the steady state solitary waves obtained here will be compared with approximate solitary wave solutions derived using modulation theory [15].

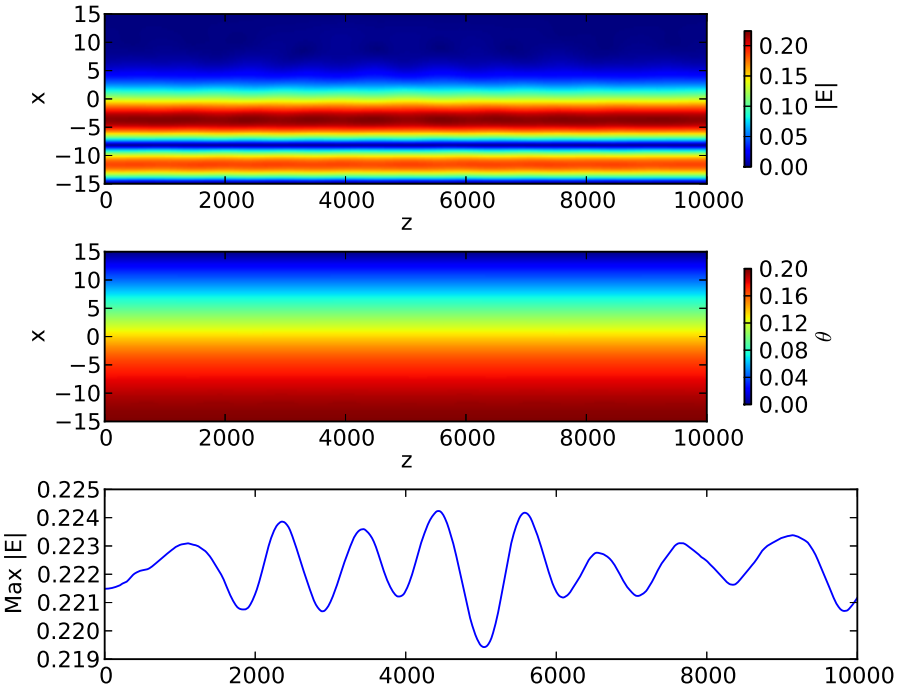

Figure 14. (Colour online) Numerical solutions of (1) and (2). Shown are the electric field $|E|$ and temperature θ in the (x, z) plane, and the maximum value of $|E|$, versus z, up to $z = 10000$. The parameters are $\mu = 0.28$, $\theta_B = 0.2$, $\beta = 100$ and $\nu = 100$. Upper panel: $|E|$. Middle panel: θ. Lower panel: Maximum value of $|E|$ (solid line, blue).

Acknowledgement: The authors wish to thank the anonymous referees for their valuable comments.

Appendix A. Stopping condition for the iterative solvers

Selecting a suitable discretization scheme for the iterative methods requires some care, as there is limited benefit in setting the stopping condition for the scheme at a lower level than the error introduced by the discretization. The amplitude of the solitary wave can be expanded in the series

$$a = a(\Delta x) + a_1 \Delta x^4 + O(\Delta x^6), \tag{A.1}$$

as the fourth order Runge-Kutta method is used, where a is the exact solution, $a(\Delta x)$ is the numerically derived solution and a_1 the amplitude of the fourth-order error term. Taking $\Delta x = 0.33$ and $\Delta x = 0.66$ with $\nu = 100$, $\mu = 1$, $\beta = 100$ and $\theta_B = 0.2$ yields the values $a(0.33) = 0.8338225$ and $a(0.66) = 0.8336788$, respectively. We can then derive higher order approximations to a and the leading order error a_1 on using Richardson extrapolation, as

$$a = \frac{2^2 a(0.33) - a(0.66)}{2^2 - 1} + O(\Delta x^5) \approx 0.83387 \tag{A.2}$$

$$a_1 = \frac{a(0.33) - a(0.66)}{1 - \frac{0.66}{2^2}} + O(\Delta x^5) \approx 1.72 \times 10^{-4}. \tag{A.3}$$

From these we can calculate that the discretization error when $\Delta x = 0.33$ is $a - a(0.33) \approx 4.75 \times 10^{-5}$. The stopping condition ϵ should then be less than $\mathrm{O}(10^{-5})$ and greater than the round-off error. Hence, we choose $\epsilon = 10^{-10}$, which is suitable for the choice $\Delta x = 0.33$ and also for much smaller choices of Δx.

References

[1] A. Hasegawa. *Optical solitons in fibres*, volume 116 of *Springer Tracts in Modern Physics*. Springer, Berlin, 2nd edition, 1990.

[2] A. Govind. *Nonlinear fiber optics*. Academic Press, New York, 3rd edition, 2001.

[3] Y. Kivshar and G. Agrawal. *Optical Solitons: From Fibers to Photonic Crystals*. San Diego. Academic, 2003.

[4] C. Conti, M. Peccianti, and G. Assanto. Route to nonlocality and observation of accessible solitons. *Phys. Rev. Lett.*, 91(073901), 2003.

[5] E.W. Dubby and J.R. Whinnery. Thermal self-focusing of laser beams in lead glasses. *Appl. Phys. Lett.*, 13:284–286, 1968.

[6] A.G. Litvak. Self-focusing of powerful light beams by thermal effects. *JETP Lett.*, 4:230–233, 1966.

[7] A.G. Litvak, V.A. Mironov, G.M. Fraiman, and A.D. Yunakovskii. Thermal self-effect of wave beams in a plasma with a nonlocal nonlinearity. *Fiz. Plazmy*, 1:60–71, 1975.

[8] E. Kuznetsov, A. Rubenchik, and V. Zakharov. Soliton stability in plasmas and hydrodynamics. *Phys. Rep.*, 142(3):103–165, 1986.

[9] C. Rotschild, O. Cohen, O. Manela, M. Segev, and T. Carmon. Solitons in nonlinear media with an infinite range of nonlocality: First observation of coherent elliptic solutions and vortex ring solutions. *Phys. Rev. Lett.*, 95(213904), 2005.

[10] C. Rotschild, B. Alfassi, O. Cohen, and M. Segev. Long-range interactions between optical solitons. *Nature Phys.*, pages 769–774, 2006.

[11] I. Khoo. *Liquid Crystals*. Wiley Interscience, Hoboken, 2007.

[12] G. Assanto, M. Peccianti, and C. Conti. Nematicons: Optical spatial solitons in nematic liquid crystals. *Optics and Photonics News*, 14(2):44–48, 2003.

[13] A.B. Aceves, J.V. Moloney, and A.C. Newell. Theory of light-beam propagation at nonlinear interfaces. i equivalent-particle theory for a single interface. *Phys. Rev. A*, 39:1809–1827, 1989.

[14] O. Bang, W. Krolikowski, J. Wyller, and J. Rasmussen. Collapse arrest and soliton stabilization in nonlocal nonlinear media. *Phys. Rev. E*, 66(4), 2002.

[15] A.A. Minzoni, N.F. Smyth, and A.L. Worthy. Modulation solutions for nematicon propagation in nonlocal liquid crystals. *J. Opt. Soc. Am. B*, 24:1549–1556, 2007.

[16] C. Conti, M. Peccianti, and G. Assanto. Observation of optical spatial solitons in a highly nonlocal medium. *Phys. Rev. Lett.*, 92(113902), 2004.

[17] C. Barsi, W. Wan, C. Sun, and J. Fleischer. Dispersive shock waves with nonlocal nonlinearity. *Opt. Lett.*, 32:2930–2932, 2007.

[18] C. Conti, A. Fratalocchi, M. Peccianti, G. Ruocco, and S. Trillo. Observation of a gradient catastrophe generating solitons. *Phys. Rev. Lett.*, 102(083902), 2009.

[19] N. Ghofraniha, C. Conti, G. Ruocco, and S. Trillo. Shocks in nonlocal media. *Phys. Rev. Lett.*, 99(043903), 2007.

[20] A. Yakimenko, Y. Zaliznyak, and Y.S. Kivshar. Stable vortex solitons in nonlocal self-focusing nonlinear media. *Phys. Rev. E*, 71(065603), 2005.

[21] A.A. Minzoni, N.F Smyth, A.L. Worthy, and Y.S. Kivshar. Stabilization of vortex solitons in nonlocal nonlinear media. *Phys. Rev. A*, 76(063803), 2007.

[22] A. Alberucci and G. Assanto. Propagation of optical spatial solitons in finite-size media: interplay between nonlocality and boundary conditions. *J. Opt. Soc. Am. B*, 24:2314–2320, 2007.

[23] A. Alberucci, M. Peccianti, and G. Assanto. Nonlinear bouncing of nonlocal spatial solitons at the boundaries". *Opt. Lett.*, 32:2795–2797, 2007.

[24] A.A. Minzoni, L.W. Sciberras, N.F. Smyth, and A.L. Worthy. Propagation of optical spatial solitary waves in bias-free nematic-liquid-crystal cells. *Phys. Rev. A*, 84(043823), 2011.

[25] B. Alfassi, C. Rotschild, O. Manela, M. Segev, and D. Christodoulides. Boundary force effects exerted on solitons in highly nonlocal media. *Opt. Lett.*, 32:154–156, 2007.

[26] A. Alberucci, G. Assanto, D. Buccoliero, A. Desyatnikov, T.R. Marchant, and N.F Smyth. Modulation analysis of boundary-induced motion of optical solitary waves in a nematic liquid crystal. *Phys. Rev. A*, 79(043816), 2009.

[27] A. Snyder and D.J. Mitchell. Accessible solitons. *Science*, 276(5318):1538–1541, 1997.

[28] T.R. Marchant and N.F. Smyth. Solitary waves and their stability in colloidal media: Semi-analytical solutions. *Dyn. Cont. Disc. Impul. Sys.*, 19:525–541, 2012.

[29] G.B. Whitham. *Linear and nonlinear waves.* J. Wiley and Sons, New York, 1974.

[30] D. Anderson. Variational approach to nonlinear pulse propagation in optical fibers. *Phys. Rev. A*, 27:3135–3145, 1983.

[31] G. Assanto, A.A. Minzoni, M. Peccianti, and N.F. Smyth. Optical solitary waves escaping a wide trapping potential in nematic liquid crystals: Modulation theory. *Phys. Rev. A*, 79(033837), 2009.

[32] G. Assanto, N.F Smyth, and W. Xia. Modulation analysis of nonlinear beam refraction at an interface in liquid crystals. *Phys. Rev. A*, 84(033818), 2011.

[33] P.D. Rasmussen, O. Bang, and W. Krolikowski. Theory of nonlocal soliton interaction in nematic liquid crystals. *Phys. Rev. E*, 72(066611), 2005.

[34] J. Yang and T.I. Lakoba. Universally-convergent squared operator iteration methods for solitary waves in general nonlinear wave equations. *Stud. Appl. Math.*, 118:153–197, 2007.

[35] J. Yang and T.I. Lakoba. Accelerated imaginary-time evolution methods for the computation of solitary waves. *Stud. Appl. Math.*, 120:265–292, 2008.

[36] J. Yang. Newton-conjugate-gradient methods for solitary wave computations. *J. Comp. Phys.*, 228:7007–7024, 2009.

[37] J. P. Boyd. Why Newton's method is hard for travelling waves: Small denominators, KAM theory, Arnold's linear Fourier problem, non-uniqueness, constraints and erratic failure. *Math. Comput. Simul.*, 74(2-3):72–81, 2007.

[38] H. Wang. Numerical studies on the split-step finite difference method for nonlinear schrodinger equations. *App. Math. Comp.*, 170, 2005.

[39] A. Alberucci, A. Piccardi, M. Peccianti, M. Kaczmarek, and G. Assanto. Propagation of spatial optical solitons in a dielectric with adjustable nonlinearity. *Phys. Rev. A*, 82, 2010.

[40] J.R. Douglas and H.H. Rachford. On the numerical solution of heat conduction problems in two and three space variables. *Tr. A.M.S.*, 82(2):421–439, 1956.

[41] T.R. Marchant and N.F. Smyth. Nonlocal validity of an asymptotic one dimensional nematicon solution. *J. Phys A.:Math. Theor.*, 41(365201), 2008.

[42] R.H. Enns and S.S. Rangnekar. Bistable-soliton pulse propagation. *Phys. Rev. A*, 36(3), 1987.

[43] A.E. Kaplan. Bistable solitons. *Phys. Rev. Lett.*, 55(12):1291–1294, 1985.

[44] A.E. Kaplan. Robust bistable solitons of the highly nonlinear shrodinger equation. *Phys. Rev. A.*, 35(1):455–469, 1987.

[45] G. Assanto, T.R. Marchant, A.A. Minzoni, and N.F. Smyth. Reorientational versus Kerr dark and grey solitary waves using modulation theory. *Phys. Rev. E.*, 84(6), 2011.